Progress In Electromagnetics Research C, Vol. 12, 65–77, 2010

PARAMETRIC STUDIES ON THE CIRCULARLY POLARIZED STACKED ANNULAR-RING MICROSTRIP ANTENNA

X. Chen, G. Fu, S. X. Gong, Y. L. Yan, and J. Chen

National Key Lab. of Antenna and Microwave Technology
Xidian University
Xi'an 710071, China

Abstract—In this paper, we propose a circularly polarized (CP) stacked annular-ring microstrip antenna (SARMSA) with an integrated feeding network in the UHF RFID band. A circular parasitic patch is suspended above the annular ring to improve the impedance matching and bandwidth. Through the parametric studies on SARMSA, the CP characters of the entire antenna are well understood, and an optimized CP character is obtained. Prototypes are fabricated to confirm the theoretical results. The experimental results indicate the impedance bandwidth for $S_{11} < -10$ dB is 870–967 MHz (10.6% at 915 MHz), and the 3 dB AR bandwidth is 893–948 MHz (6%). Meanwhile, the measured CP gain reaches 8.9 dBic at 915 MHz.

1. INTRODUCTION

Rectangular and circular patch microstrip antennas are traditionally used to implement circular polarization [1, 2]. In recent years, annular-ring microstrip antenna (ARMSA) is another available structure to realize circular polarization [3–11]. It can be achieved by cutting a concentric circular slot on the circular radiating patch. At a fixed operating frequency, an annular-ring patch can realize more miniature dimensions than that of a circular patch, which is because the behavior of slotting on the patch extends the path of current flowing [12]. The CP operation of the annular ring also involves introducing perturbation segments [3, 4] or adding feeding network [10, 11]. However, the very large input impedance of ARMSA is an obstacle when an annular ring works in TM_{11} and TM_{21} modes [13]. In the literatures, some

Corresponding author: X. Chen (chenxi1223@gmail.com).

techniques have been proposed to solve this problem. In [3], the authors use microstrip line as impedance transformer to realize matching with the characteristic impedance of 50 Ω. In [4–8], the technique of coupling feeding is used to improve the impedance matching. Loading gaps, slits, or stubs on the ring is another method to be involved [9], but the patch mainly works at linear polarization, and polarization rotation can be caused by the loading. However, the above approaches hardly provide wide impedance bandwidth because of the single resonant frequency. Stacking parasitic patch above the annular ring can greatly reduce the value of input impedance [10, 11], and the bandwidth can be broadened obviously due to exciting two adjacent resonant frequencies. But in [10], the authors did not provide the relative parametric studies on the antenna performance, especially, the CP performance when the antenna works in circular polarization.

In this paper, we design a CP stacked annular-ring microstrip antenna (SARMSA) working in TM_{11} mode. The CP character is implemented by an integrated power divider. The parameters of the ARMSA are studied in detail since they have a significant effect on the performance of the proposed antenna. The experimental results are provided to verify the correctness of the analysis.

2. ANTENNA CONFIGURATION

The configuration of the proposed antenna is shown in Fig. 1(a). The main components involve a circular parasitic patch, a printed circuit broad (PCB) with an annular ring and a feeding network on it, and a square metallic ground. The annular ring with inner radius a and outer radius b is etched on a circular substrate with radius $R_s = 55\,\text{mm}$ (0.168λ at 915 MHz) and thickness $t_s = 1\,\text{mm}$ (0.003λ). For the consideration of low cost, PTFE with relative permittivity $\varepsilon_r = 2.65$ is selected as the substrate material. At the inner of the ring, a reshaped equal-split power divider is also etched on the top surface of the substrate. For the size reduction of the feeding network and the smoothness of the microstrip lines, Archimedes gradual-change lines are used to construct branch lines of the divider. Fig. 1(b) is the local view of the feeding network. The length of the branch 1 is about $\lambda_g/4$ and controlled by r_1 and r_2, where λ_g is the guided wavelength, while the length of the branch 2 is about $\lambda_g/2$ and controlled by r_3 and r_4. The segment adjusting 90° phase shift is controlled by its corresponding central angle θ. The widths w_1 and w_2 of the microstrip lines determine their characteristic impedances of 70 Ω and 50 Ω respectively. In this application, the isolation resistor is omitted, so the insert loss of the network is small. To improve the impedance matching and bandwidth

of the annular ring, we suspend a 0.8 mm-thickness circular parasitic patch above the PCB at the height h. When the diameter of the patch is about a half wavelength in free space, a good radiation feature can be obtained. The square metallic ground is attached to the bottom surface of the substrate, and its size has an obvious effect on the gain and the ratio of front to back (F/B) but less effect on the impedance and AR bandwidths. After adjustment and optimization based on the initial sizes, the designed parameters are fixed as $a = 25.8$ mm, $b = 42.6$ mm, $d_r = 167.9$ mm (0.51λ), $h = 10$ mm (0.03λ), $r_1 = 17$ mm, $r_2 = 22$ mm, $r_3 = 17$ mm, $r_4 = 25$ mm, $w_1 = 1.3$ mm, $w_2 = 2.4$ mm, $\theta = 120^\circ$, and $L_g = 220$ (0.67λ).

Figure 2 shows the power distribution ratio and phase difference of the designed feeding network when the output ports connect to 50 Ω. It is observed that a good CP character is provided. Since the character of power divider is widely known, its parametric studies are not performed here. In the following sections, the parameters of the SARMSA are studied in detail for understanding the performance of the entire antenna. The commercial software HFSS is used to guide the studies.

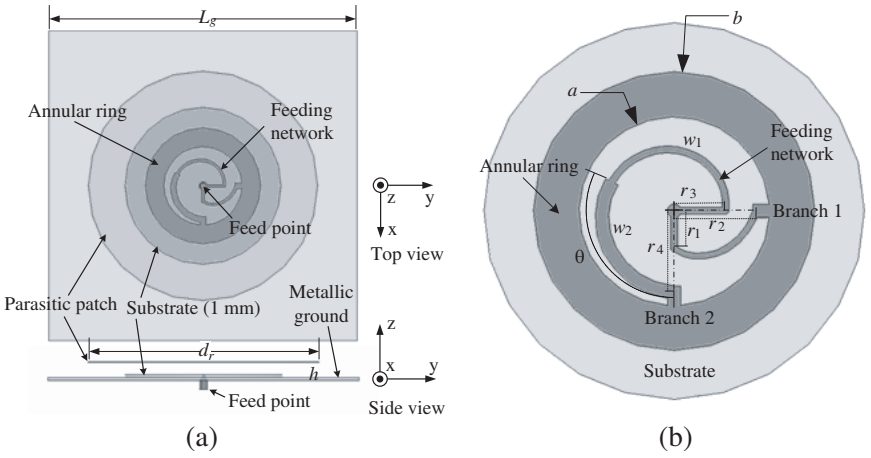

Figure 1. Configurations of the proposed antenna. (a) Full view. (b) Local view.

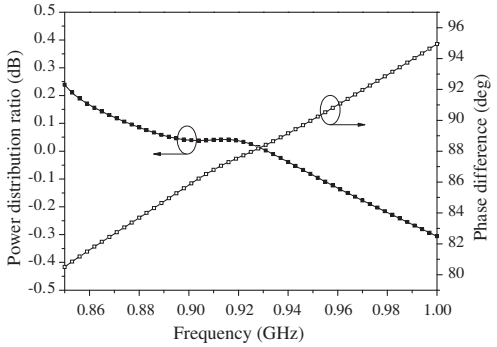

Figure 2. Power distribution ratio and phase difference of the proposed feeding network at output ports.

3. PARAMETRIC STUDIES

3.1. ARMSA

ARMSA is the foundation of the proposed antenna. The character of ARMSA has been studied in theory and practice [13–16]. In practical applications, its resonant frequency, input impedance, and impedance bandwidth are the keys to be concerned. In general, when the annular-ring patch works in TM_{11} mode, the resonant frequency can be expressed as [4]

$$f_{11} = \frac{c}{\pi(a+b)\sqrt{\varepsilon_{eff}}} \tag{1}$$

where c is the speed of light in free space, $\pi(a + b)$ the mean circumferential length of the annular-ring patch, and ε_{eff} the effective permittivity. Obviously, when the material and sizes of the substrate iare fixed, the resonant frequency is determined by a and b. Figs. 3(a) and (b) show the simulated resonant frequency and input resistance versus the ratio of a to b (a/b) with two different substrate thicknesses, where the outer radius b is fixed at 42.6 mm. It illustrates, at a fixed frequency, the thinner substrate has lower resonant frequency and smaller input impedance than that of the thicker one. In addition, Fig. 3(b) also indicates that as the width of the annular ring increases, i.e., a/b decreases, the input impedance drops dramatically. According to this rule, we can change a and b jointly to adjust the value of input impedance greatly at a fixed frequency. The precise sizes of a and b are decided by the value of input impedance and its bandwidth after stacking the parasitic patch. We select $a = 25.8$ mm as designing parameter, i.e., $a/b = 0.6$. The resonant frequency and the input impedance of the ARMSA are recorded in Table 1.

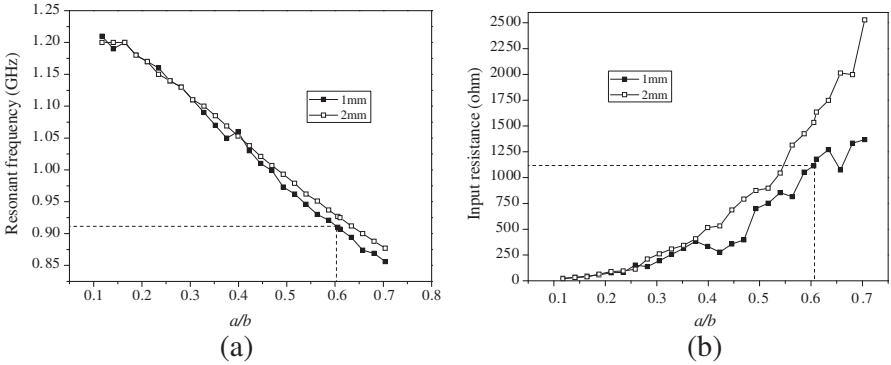

Figure 3. Simulated characters on ARMSA versus a/b with different substrate thickness. —■— 1 mm, —□— 2 mm. (a) Resonant frequency. (b) Input impedance.

Table 1. Comparison of resonant characters between ARMSA and SARMSA.

Characters / Types	f/MHz		R_{in}/Ω	
ARMSA	910		1114	
SARMSA	892	948	68	60

3.2. SARMSA

Stacking a parasitic patch above the annular ring has been used to improve the impedance matching [10, 11]. However, we have not seen the relative studies on the relationships between the parameters of the parasitic patch and the characters of SARMSA, especially, the impedance matching, impedance bandwidth, AR value, and AR bandwidth when the antenna works in circular polarization by a feeding network. Therefore, to illustrate the relationships between the SARMSA and entire antenna, we present the parametric studies of the parasitic patch in detail below. To accurately understand the effect of these critical parameters on the input impedance and AR performance, the sizes of the annular ring and the feeding network are fixed as those mentioned in Section 2.

(1) The diameter of the parasitic patch — d_r.

Figure 4 shows the impedance loci of the SARMSA with the parasitic patch of different diameters d_r, as well as no parasitic patch. First, it indicates that after stacking parasitic patch, the impedance

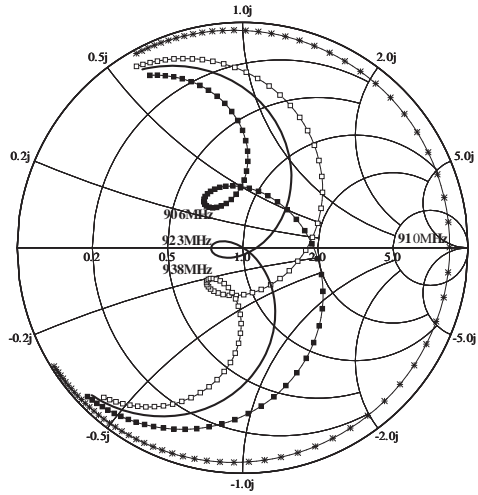

Figure 4. Impedance loci of ARMSA with various dr. —□— $d_r = 165\,\text{mm}$, — $d_r = 167.9\,\text{mm}$, —■— $d_r = 171\,\text{mm}$, —×— no parasitic patch.

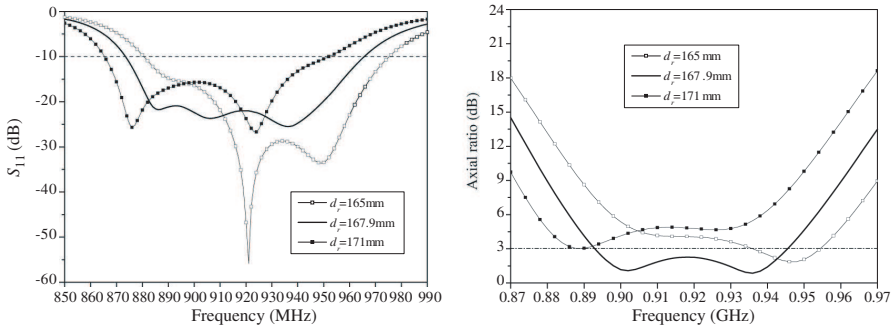

Figure 5. S_{11} and AR on the entire antenna with various d_r. (a) S_{11}. (b) AR.

matching is improved remarkably in a wide band, i.e., a loop is formed on impedance loci. When $d_r = 167.9\,\text{mm}$, two adjacent resonant frequencies are excited simultaneously around 915 MHz. The frequencies and their input resistances are also recorded in Table 1 for comparing. In fact, the middle frequency of the two resonant frequencies decides the single resonant frequency of the ARMSA, and the values of the input resistance decide that of the ARMSA. Accordingly, the sizes of a and b are determined in this way. Secondly,

as the diameter decreasing, the loop is transformed from capacitive character to inductive one, while the dimension of the loop changes little. It implies a stable impedance bandwidth. Meanwhile, the middle point of the two resonant frequencies is shifted toward lower frequency. Figs. 5(a) and (b) show the variations of S_{11} and AR of the entire antenna respectively for different d_r. It is observed that both of the performances express frequency shift versus d_r. The impedance bandwidth for $S_{11} < -10\,\text{dB}$ changes slightly as that of the SARMSA, and the AR bandwidth is also maintained. However, the values of S_{11} and AR degenerate totally or partially. This point is easy to be ignored in the study of linear polarization.

(2) The height between parasitic patch and annular ring — h.

Figure 6 shows the impedance loci of SARMSA for various heights h between the parasitic patch and annular ring. It is observed that except for a little change on the character of reactance, the impedance bandwidth increases as the height decreases, i.e., the impedance loop becomes a large one from a point. For the entire antenna, the impedance and AR bandwidth, shown in Fig. 7, are also enhanced by reducing h, e.g., the impedance bandwidth of $h = 8\,\text{mm}$ is 15.2% wider than that of $h = 10\,\text{mm}$. It is beneficial for linear polarization. But its AR values exceed 3 dB partially. In contrary, the case of $h = 11\,\text{mm}$ has a good AR value in a smaller bandwidth. It is indicated that a good impedance matching of the SARMSA can cause a lower AR value but a narrower AR bandwidth.

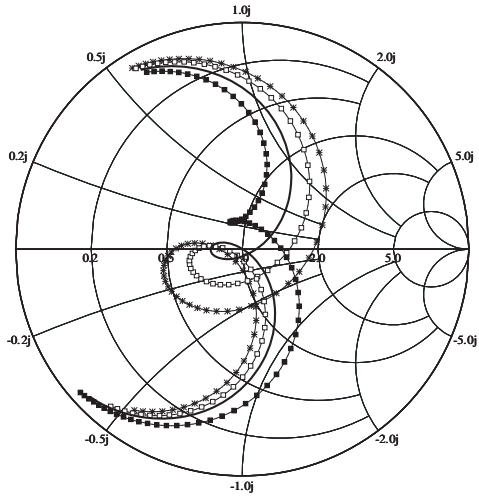

Figure 6. Impedance loci of ARMSA with various h. —×— $h = 8\,\text{mm}$, —□— $h = 9\,\text{mm}$, — $h = 10\,\text{mm}$, —■— $h = 11\,\text{mm}$.

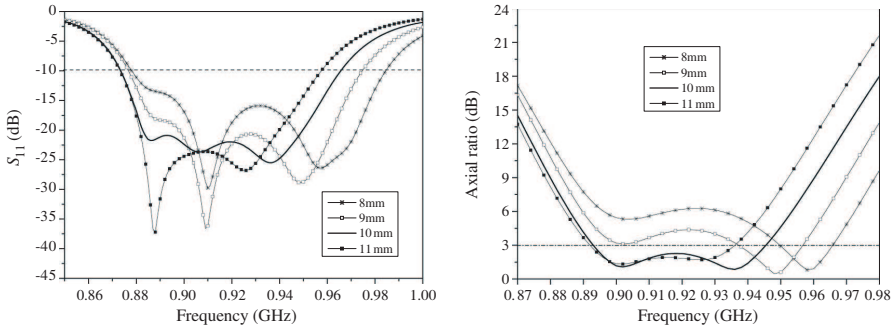

Figure 7. S_{11} and AR on the entire antenna with various h. (a) S_{11}. (b) AR.

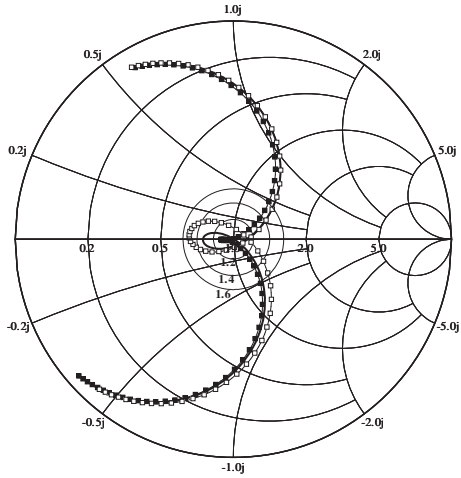

Figure 8. Impedance loci of ARMSA with three groups of h and d_r. —□— $h = 9.3\,\text{mm}$, $d_r = 168.6\,\text{mm}$, — $h = 10\,\text{mm}$, $d_r = 167.9\,\text{mm}$, —■— $h = 11\,\text{mm}$, $d_r = 166.1\,\text{mm}$.

According to the results above, we have a consideration of d_r and h in common to obtain different characteristics of the entire antenna. Fig. 8 illustrates three impedance loci of the ARMSA according to three groups of d_r and h. Several equal-VSWR circles are drawn on the Smith chart for reference. And the corresponding S_{11} and AR of the entire antenna are shown in Fig. 9. It is observed that when $h = 11\,\text{mm}$ and $d_r = 166.1\,\text{mm}$, the impedance loci form a point in the circle of VSWR < 1.2, but the bandwidth of the ARMSA is narrow. In this case, the entire antenna has good AR values, which are less than 1.68 dB from 896 MHz to 938 MHz. When $h = 9.3\,\text{mm}$ and

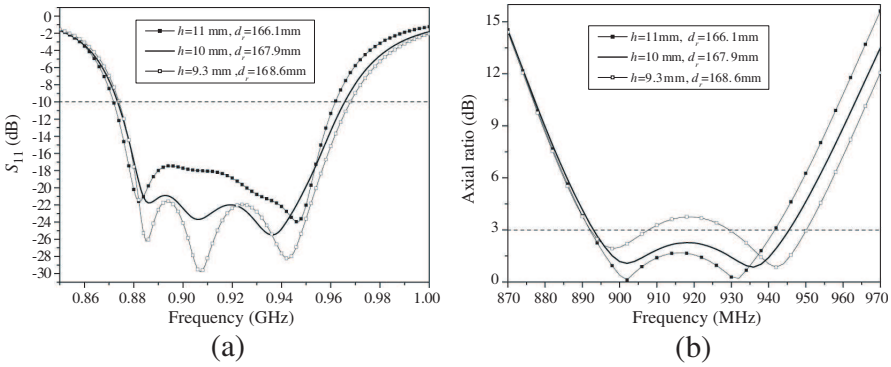

Figure 9. S_{11} and AR on the entire antenna with three groups of h and d_r. (a) S_{11}. (b) AR.

$d_r = 168.6$ mm, the entire antenna forms two 3 dB AR bandwidth apart from 45 MHz. Here, the impedance loop of the ARMSA is in the circle of VSWR < 1.6. A good compromise on the AR value and bandwidth can be obtained when $h = 10$ mm and $d_r = 167.9$ mm, and its impedance loop of ARMSA is in the circle of VSWR < 1.4. It is noted from the Fig. 9(a) that the impedance bandwidth for $S_{11} < -10$ dB has a small change with the three groups' sizes. The experimental results are mainly attributed to the condition of impedance matching between the ARMSA and feeding network. Due to no isolation resistor in the feeding network, the equal-power distribution is satisfied well in the case of good impedance matching between the ARMSA and feeding network. But for SARMSA, as shown in Fig. 8, the values of input impedance and its bandwidth are contradictive. Therefore, lower AR values and wider AR bandwidth cannot be obtained together, but we can obtain the ARMSA with high CP purity or dual-frequency CP character respectively in terms of demands.

4. EXPERIMENTAL RESULTS AND DISCUSSIONS

According to the conclusions of the parametric studies, we fabricate prototypes with $h = 10$ mm and $d_r = 167.9$ mm for a balanced consideration. Their photos are shown in Fig. 10. The measured S_{11}, compared with simulated values, is shown in Fig. 11. The measurements are implemented in an Aglient network analyzer E8363B. As shown in the figure, the measured impedance bandwidth for $S_{11} < -10$ dB is 870–967 MHz (10.6% at 915 MHz), and it agrees well with the simulated one despite of a little higher S_{11} values. It is mainly due to the manufacture tolerances, e.g., the state of the soldering causes the change of the input impedance.

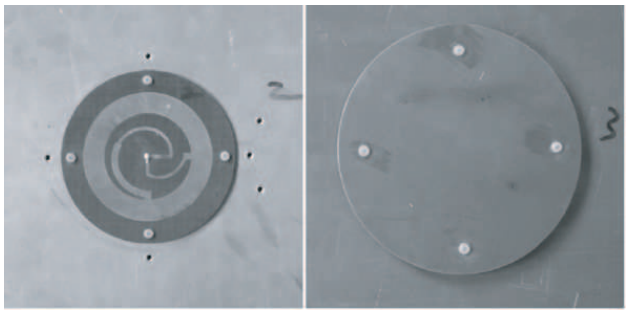

Figure 10. Photos of the proposed antenna.

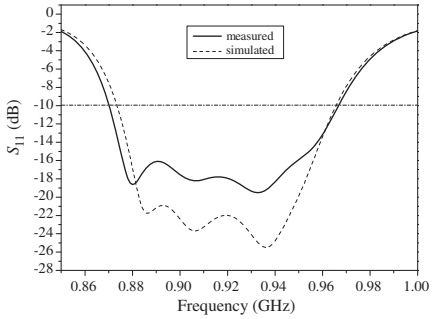

Figure 11. Measured and simulated S_{11}.

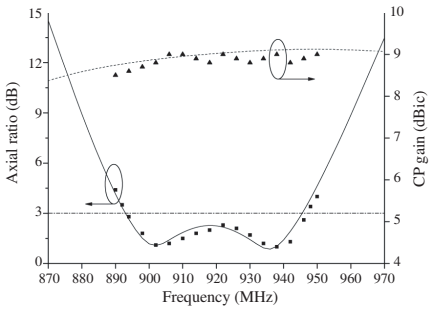

Figure 12. Measured and simulated AR and CP gain. — simulated AR, ■ measured AR, – – – simulated CP gain, ▲ measured CP gain.

Figure 12 shows the measured CP gain and AR of the proposed antenna compared with the simulated results at broadside direction. The measured values of AR and CP gain are both derived from the two orthogonal linearly polarized vectors measured by a standard gain horn antenna [17]. It is observed that the measured 3 dB AR bandwidth is 893–948 MHz (6% at 915 MHz), and the values shift toward high frequency slightly compared with the simulated one. The CP gain in this band also agrees with the simulated values in spite of some disturbance. It is also observed that the gain of 8.9 dBic is obtained at 915 dBic, and the gain is more than 8.5dBic from 893 MHz to 948 MHz. It is noted that the proposed antenna has better radiation features and smaller ground sizes than those in recent literatures [6, 7]. Furthermore, if we could sacrifice some radiation capability, i.e., gain and F/B, smaller antenna dimensions could be achieved.

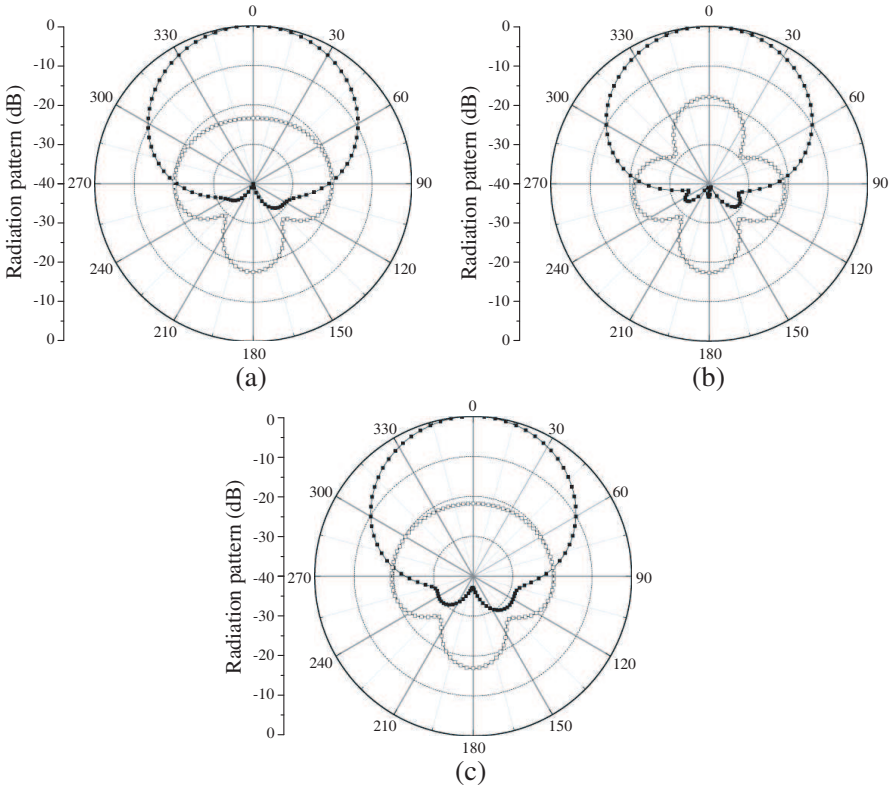

Figure 13. Simulated CP radiation patterns in x-z plane. —■— LHCP, —□— RHCP. (a) At 900 MHz, F/B = −17.6 dB, HPBW = 65°. (b) At 915 MHz, F/B = −17.4 dB, HPBW = 64°. (c) At 940 MHz, F/B = −16.9 dB, HPBW = 64°.

Due to the limitation of measurements, the measured circularly polarized radiation patterns (RP) are not acquired. But from the agreement of CP gain between measurement and simulation, it is believed that the simulated data have the value of reference. The simulated CP RP in x-z plane at 900 MHz, 915 MHz, and 940 MHz are provided separately in Fig. 13. The F/Bs and the half power beam widths (HPBW) are listed below the figures.

5. CONCLUSION

A CP stacked annular-ring microstrip antenna with an integrated feeding network is proposed in this paper. Parametric studies are performed on the SARMSA to illustrate the CP characters of the

proposed antenna. For the proposed antenna, different CP characters can be obtained in terms of the condition of the parasitic patch. Prototypes are fabricated to confirm the theoretical studies. The experimental results agree well with the simulated ones, and it is indicated that the impedance bandwidth for $S_{11} < -10$ dB is 870–967 MHz, 10.6% at 915 MHz, and the 3 dB AR bandwidth is 893–948 MHz, 6% at 915 MHz. The overlapped bandwidth can well cover American UHF RFID band, i.e., 902–928 MHz. Meanwhile, the measured CP gain can reach 8.9 dBic at 915 MHz.

REFERENCES

1. Kasabegoudar, V. G. and K. J. Vinoy, "A broadband suspended microstrip antenna for circular polarization," *Progress In Electromagnetics Research*, PIER 90, 353–368, 2009.
2. Yang, S. L. S., K. F. Lee, and A. A. Kishk, "Design and study of wideband single feed circularly polarized microstrip antennas," *Progress In Electromagnetics Research*, PIER 80, 45–61, 2008.
3. Chen, H. M. and K. L. Wong, "On the circular polarization operation of annular-ring microstrip antennas," *IEEE Trans. Antennas Propag.*, Vol. 47, No. 8, 1289–1292, 1999.
4. Lin, Y. F., H. M. Chen, and S. C. Lin, "A new coupling mechanism for circularly polarized annular-ring patch antenna," *IEEE Trans. Antennas Propag.*, Vol. 56, No. 1, 11–16, 2008.
5. Row, J. S., "Design of aperture-coupled annular-ring microstrip antennas for circular polarization," *IEEE Trans. Antennas Propag.*, Vol. 53, No. 5, 1779–1784, 2005.
6. Tong, K. F. and J. J. Huang, "New proximity coupled feeding method for reconfigurable circularly polarized microstrip ring antennas," *IEEE Trans. Antennas Propag.*, Vol. 56, No. 7, 1860–1866, 2008.
7. Guo, Y. X., L. Bian, and X. Q. Shi, "Broadband circularly polarized annular-ring microstrip antenna," *IEEE Trans. Antennas Propag.*, Vol. 57, No. 8, 2474–2477, 2009.
8. Ridgers, G. M., J. W. Odendaal, and J. Joubert, "New feeding mechanism for annular-ring microstrip antenna," *Electron. Lett.*, Vol. 36, No. 7, 605–606, 2000.
9. Latif, S. I. and L. Shafai, "Polarization characteristic of multiband loaded microstrip annular ring antennas," *IEEE Trans. Antennas Propag.*, Vol. 57, No. 7, 2788–2793, 2009.
10. Al-Charchafchi, S. H., W. K. Wan Ali, and S. Sinkeree, "A stacked

annular-ring microstrip patch antenna," *IEEE APS International Symposium Digest*, Vol. 2, 948–951, 1997.

11. Ohmine, H., Y. Sunahara, and M. Matsunaga, "An annular-ring microstrip antenna fed by a co-planar feed circuit for mobile satellite communication use," *IEEE Trans. Antennas Propag.*, Vol. 45, No. 6, 1001–1008, 1997.
12. Wu, Y. S. and F. J. Rosenbaum, "Mode chart for microstrip ring resonators," *IEEE Trans. Microwave Theory Tech.*, Vol. 21, 487–489, 1973.
13. Liu, H. and X. F. Hu, "Input impedance analysis of a microstrip annular-ring antenna with a thick substrate," *Progress In Electromagnetics Research*, PIER 12, 177–204, 1996.
14. Chew, W. C., "A broad-band annular-ring microstrip antenna," *IEEE Trans. Antennas Propag.*, Vol. 30, No. 5, 918–922, 1982.
15. Lee, K. F. and J. S. Dahele, "Theory and experiment on the annular-ring microstrip antenna," *Annals of Telecommunications*, Vol. 40, 508–515, 1985.
16. Dahele, J. S., K. F. Lee, and D. P. Wong, "Dual-frequency stacked annular-ring microstrip antenna," *IEEE Trans. Antennas Propag.*, Vol. 35, No. 11, 1281–1285, 1987.
17. Lo, Y. T. and S. W. Lee, *Antenna Handbook*, Chapman and Hall, New York, NY, 1993.